

# GAIT ANALYSIS OF A FREE-CLIMBING ROBOT ON SLOPED TERRAIN FOR LUNAR AND PLANETARY EXPLORATION

\*Yuki Shirai<sup>1</sup>, Hayato Minote<sup>1</sup>, Kenji Nagaoka<sup>1</sup>, and Kazuya Yoshida<sup>1</sup>

<sup>1</sup> Tohoku University, 6-6-01 Aoba, Aramaki, Aoba-ku, Sendai, Miyagi, Japan  
E-mail: {shirai, minote, nagaoka, yoshida}@astro.mech.tohoku.ac.jp

## ABSTRACT

In this paper, we discuss free-climbing gaits on sloped terrains based on tumble stability margin and manipulability in a quantitative way. The tumble stability margin considers a tumbling moment according to forces and moments acting on a robot with legs, and the manipulability considers the movements of the legs. Considering these parameters, we propose a more suitable gait called hybrid gait for slope walking. Hybrid gait increases the tumble stability margin by shifting the main body of the robot to improve stability during slope walking. To validate the proposed gait, we conducted numerical simulations and experiments using a prototype robot. The result shows that although the robot overturns during different gaits, such as adaptive gait and sway compensation gait, it does not tumble when using the hybrid gait on sloped terrain. Our findings confirm that the proposed gait achieves the most stable locomotion on slopes.

## 1 INTRODUCTION

Recently, the use of mobile robots for lunar and planetary exploration has received attention because these robots provide a possible means for conducting more challenging missions. In particular, lunar lava tubes, including steep cliff walls, have attracted a great deal of attention from scientific interests and as a future habitat for humans [1]. Although NASA's wheeled rovers have achieved robotic exploration on the Martian surface, it is extremely difficult for them to access areas like rock outcrops. For example, the Mars Exploration Rover, Opportunity, tried to examine layering in the rock outcrops of Victoria Crater, for these stratified layers help us to understand the geologic history of the site. Despite NASA's efforts, Opportunity could not access the layering and gave up deploying its scientific instruments as the slopes were too steep [2]. Hence, in order for a robot to access these kinds of complicated environments, free-climbing capabilities on cliff walls are required. As shown in Figure 1, we have proposed a free-climbing robot moving on a cliff by gripping its surface for robotic exploration [3]. NASA has also developed free-climbing robots, and the latest model, LEMUR 3 [4], is a quadruped robot with a microspine gripper on each leg. It demonstrated free-climbing motion on natural cliff walls.

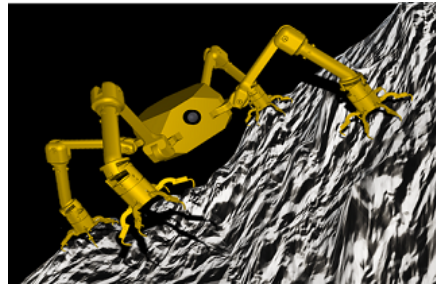


Figure 1: Conceptual drawing of a free-climbing robot

In order for a free-climbing robot to maintain climbing motion on a cliff face, gait control is necessary for better stability. It is also important to evaluate the stability of the robot on irregular terrains based on suitable stability criteria. In the past, research on walking robot was the standard for evaluating static stability and used the relation between the support leg polygon, which is created by connecting the points of the support leg touching the ground, and the projected point of the center of gravity on the ground. However, this standard does not consider external forces and moments acting on the robot, such as the force of the gripper. In addition, the zero moment point (ZMP) has been used for evaluating dynamic stability criteria [5]. However, the concept of the ZMP targets walking on flat terrain; thus, it cannot be applied as a criterion of dynamic stability on rough rocky terrain. To overcome these issues, previous research has proposed tumble stability, which considers the tumble direction of the robot when all ground contact points, except two remaining contact points, are hypothetically lost [6]. If a given point among the ground contact points that have been hypothetically lost can produce a support force to suppress that tumble, the walking robot will not tumble. Although the tumble stability margin is used as a criterion of tumble stability and it can be used on rocky terrains, limited research studies have taken advantage of the tumble stability margin in real robot experiments. Moreover, when the legged robot walks, whether the robot can realize the intended walking motion depends on the reachable area of the leg. Hence, manipulability as a criterion of the reachable area should be taken into consideration.

In this study, we compare and analyze the tumble stability of various gaits based on the tumble stability margin

and manipulability. We then propose a more suitable gait for sloped terrains. To validate the proposed gait, we conducted numerical simulations and experiments using a prototyped robot. Furthermore, appropriate leg link parameters for free-climbing are discussed, which will be an effective benchmark for design optimization.

## 2 STABILITY MODEL OF QUADRUPED ROBOT

A typical gait stability analysis of a walking robot is based on the ZMP. This standard can be basically applied to a walking robot on a horizontal surface. However, as the ZMP does not target walking on irregular terrain, one is required to use a standard for evaluating dynamic stability on rocky terrain. In addition, the free-climbing robot requires a specialized gripper to tightly hold the terrain surface, whereas most walking robots simply equip frictional spheres or circular plates on their leg tips. The walking criterion including the gripper effects is therefore necessary for the free-climbing.

This section first introduces the concept of tumble stability and its standard called tumble stability margin. We also describe the manipulability of a legged robot.

### 2.1 Tumble Stability Margin

In this study, we focus on the static walking of a legged robot. From the view of lunar and planetary exploration, a reliable robot is necessary in unknown or uncertain environments. Hence, we discuss static walking when the static stability of a robot is always maintained. In this regard, however, an inertial force acts on the robot even when the robot walks statically. Accordingly, in this study, we evaluate the dynamic stability of the robot during static walking. Furthermore, a four-legged robot has the minimum number of legs required for static walking. In terms of mission cost for lunar and planetary exploration, it is desirable for the payload of the rocket to be as light as possible. We therefore analyze static walking for a four-legged robot.

This study adopts the tumble stability margin ( $T_{SM}$ ) as the criterion of tumble stability, which can be used in rough terrain and includes dynamic effects and the gripping force of the gripper. Here, we introduce  $T_{SM}$ . First, we calculate the sums of forces  $\mathbf{F}_a$  and moments  $\mathbf{M}_a$  required for acceleration and deceleration of all parts of the robot. Assuming that the walking robot is a mass concentration system of the  $L$  links, with each mass being  $m_i$  and each position vector being  $\mathbf{q}_i$ ,  $\mathbf{F}_a$  and  $\mathbf{M}_a$  are expressed as follows.

$$\mathbf{F}_a = \sum_{i=1}^L m_i \ddot{\mathbf{q}}_i \quad (1)$$

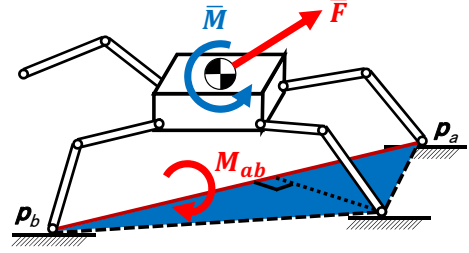


Figure 2: Conceptual diagram of tumble stability margin

$$\mathbf{M}_a = \sum_{i=1}^L m_i \mathbf{q}_i \times \ddot{\mathbf{q}}_i \quad (2)$$

The forces acting on the walking robot are gravity, reaction forces from the ground surface, and other external forces. Let  $\mathbf{F}_G$  and  $\mathbf{M}_G$  be a force and moment totaling the gravity acting on each link, and  $\mathbf{F}_0$ ,  $\mathbf{M}_0$  be a force and moment totaling the other external forces except the contact force from the ground. As shown in Figure 2, from the equilibrium of the forces, the reaction force  $\bar{\mathbf{F}}$  and moment  $\bar{\mathbf{M}}$  that should be obtained from the ground surface can be expressed as follows.

$$\bar{\mathbf{F}} = \mathbf{F}_a - \mathbf{F}_G - \mathbf{F}_0 \quad (3)$$

$$\bar{\mathbf{M}} = \mathbf{M}_a - \mathbf{M}_G - \mathbf{M}_0 \quad (4)$$

Here, if the coordinate system is the inertia coordinate system, we define the ground touching point as  $P_a, P_b, \dots, P_n$ , and the position vector to the ground touching point as  $\mathbf{p}_1, \mathbf{p}_2, \dots, \mathbf{p}_n$ . Among these, the moment  $M_{ab}$  around the line segment connecting two arbitrary ground touching points  $P_a, P_b$  can be calculated from  $\bar{\mathbf{F}}$  and  $\bar{\mathbf{M}}$ .

First,  $\bar{\mathbf{F}}$  is the translational force working on the origin of the coordinate system. The moment  $\mathbf{M}_{b\bar{\mathbf{F}}}$  around the ground touching point  $P_b$ , which is given by this translational force, is expressed as follows.

$$\mathbf{M}_{b\bar{\mathbf{F}}} = \bar{\mathbf{F}} \times \mathbf{p}_b \quad (5)$$

The magnitude of this moment around the line segment connecting the points touching the ground  $P_a, P_b$  is given as follows.

$$M_{ab\bar{\mathbf{F}}} = \mathbf{M}_{b\bar{\mathbf{F}}} \cdot \frac{(\mathbf{p}_a - \mathbf{p}_b)}{|\mathbf{p}_a - \mathbf{p}_b|} \quad (6)$$

Next,  $\bar{\mathbf{M}}$  is the moment around the origin of the coordinate system. The magnitude of this moment around the line segment connecting the points touching the ground  $P_a, P_b$  is given as follows.

$$M_{ab\bar{\mathbf{M}}} = \bar{\mathbf{M}} \cdot \frac{(\mathbf{p}_a - \mathbf{p}_b)}{|\mathbf{p}_a - \mathbf{p}_b|} \quad (7)$$

Consequently, from Eq. (6) and Eq. (7), the moment  $M_{ab}$  around the line segment connecting two arbitrary points touching the ground  $P_a, P_b$  is expressed as follows.

$$M_{ab} = \overline{M} \cdot \frac{(\mathbf{p}_a - \mathbf{p}_b)}{|\mathbf{p}_a - \mathbf{p}_b|} + \overline{F} \cdot \frac{(\mathbf{p}_b \times \mathbf{p}_a)}{|\mathbf{p}_a - \mathbf{p}_b|} \quad (8)$$

Here, it is assumed that the ground-touching points  $P_a, P_b$  have not lifted up and that the moment  $M_{ab}$  is not zero when more than two points are touching the ground. In this condition, if the direction in which the tumbling occurs is actually supported by that point, then the walking robot does not tumble so long as the moment is in the direction of one of the points touching the ground.

Here, we introduce tumble stability, which takes into consideration the gripping force of the gripper. Let the gripping force of the gripper holding the contact point  $j$  be  $F_j$ . Then, the moment generated from the gripping force that acts around the tumble axis can be expressed as follows.

$$M_{jab} = F_j \cdot \frac{(\mathbf{p}_b - \mathbf{p}_j) \times (\mathbf{p}_a - \mathbf{p}_j)}{|\mathbf{p}_a - \mathbf{p}_b|} \quad (9)$$

By considering this moment, we can express the moment working on the robot with a gripper (the free-climbing robot) around the line segment connecting two arbitrary ground-touching points  $P_a$  and  $P_b$ .

$$M_{ab} = \overline{M} \cdot \frac{(\mathbf{p}_a - \mathbf{p}_b)}{|\mathbf{p}_a - \mathbf{p}_b|} + \overline{F} \cdot \frac{(\mathbf{p}_b \times \mathbf{p}_a)}{|\mathbf{p}_a - \mathbf{p}_b|} - M_{jab} \quad (10)$$

By evaluating the moment  $M_{ab}$  on Eq. (10), it is possible to discriminate the tumble stability considering the gripping performance.

Furthermore, let  $n$  be the number of legs, and calculate the moment  $M_{ab}$  for all combinations of  $a = 1$  to  $n$ ,  $b = 1$  to  $n$ , where  $a \neq b$ . When all the determined tumble moments are cancelled by the remaining support legs, the minimum absolute value of the moment  $M_{ab}$  can be calculated. Thus, the tumble stability margin is defined as the value at which this value is further divided by the weight of the walking robot [6]. The tumble stability margin ( $T_{SM}$ ) can be expressed as follows.

$$T_{SM} = \frac{\min |M_{ab}|}{mg} \quad (11)$$

If the tumble stability is not satisfied, the tumble stability margin is set to zero. By dividing  $\min |M_{ab}|$  by the weight of the robot, the unit of the tumble stability margin becomes the dimension of length. Moreover, when the robot walks on a horizontal surface, this standard shows the same value as the ZMP. Thus,  $T_{SM}$  has continuity with the conventional standard for evaluating dynamic stability using the ZMP.

Using the tumble stability margin, it is possible to evaluate the dynamic stability of the walking robot on rough surfaces in a quantitative way.

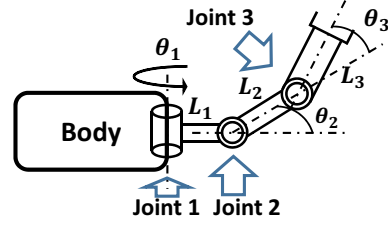


Figure 3: Kinematic definition of targeted robot

## 2.2 Manipulability

Manipulability is a criterion of the reachable area. It is important to evaluate manipulability as well as the tumble stability margin when a legged robot walks on rough ground surfaces. In addition, we can regard the legged robot as manipulators connected to a body. Once the manipulator falls into a singular point, we cannot operate it anymore. This is a particularly important problem when the robot climbs a slope. When the legged robot walks on a slope, remaining within the stable tumble stability margin is desirable. Therefore, to execute this motion, the leg sometimes falls into a singular point.

Here, we introduce manipulability. We consider an  $n$  degree of freedom leg and define a joint vector  $\theta = [\theta_1, \theta_2, \dots, \theta_n]^T$  that represents the posture of the leg. Then, the manipulability  $w$  can be expressed using Jacobian  $J(\theta)$  as follows [7].

$$w = \sqrt{\det(J(\theta)J^T(\theta))} \quad (12)$$

In this study, we analyze gaits based on the leg shown in Figure 3. In Figure 3,  $\theta_1$ ,  $\theta_2$ , and  $\theta_3$  represent the joint angles of the joints 1, 2, and 3, respectively, and  $L_1$ ,  $L_2$ , and  $L_3$  represent the lengths of the links 1, 2, and 3, respectively. The manipulability  $w$  of the target robot can be expressed as follows.

$$w = L_2 L_3 |(L_1 + L_2 C_2 + L_3 C_{23}) S_3| \quad (13)$$

where,  $C_n = \cos \theta_n$ ,  $S_Y = \sin \theta_n$ , and  $C_{nm} = \cos(\theta_n + \theta_m)$ .

## 3 HYBRID GAIT

In this section, we describe multiple gaits for slopes and propose a stable gait called hybrid gait for slope walking.

Table 1 shows parameters for each gait. Each gait analyzed in this study will be explained below with reference to its gait diagram. The gait diagrams show the time-series data of the leg tip position with respect to the center of the robot's main body.

### 3.1 Standard Gait

Here, we consider a robot walking on a horizontal plane in the  $x$  direction. Figure 4 shows the gait diagram of

Table 1: Definition of gait parameters

Parameter	Definition
$T$ [s]	Time of a gait cycle
$T'$ [s]	Time of a swing phase
$T''$ [s]	Time of a stance phase
$T'''$ [s]	Time of a quadruped support phase
$\beta$ [-]	Duty ratio: Ratio of $T''$ to $T$
$\Delta x_0$ [m]	Stride
$x_0^*$ [m]	$x$ -directional stroke
$y_0^*$ [m]	$y$ -directional stroke
$h$ [m]	Height of center of gravity from slope
$h_0$ [m]	Height of center of gravity from horizontal plane
$\theta$ [rad]	Slope angle
$\mu$ [-]	Coefficient of static friction

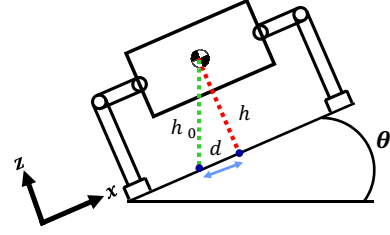


Figure 5: Robot standing on a slope

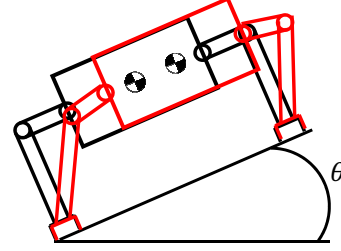


Figure 6: Adaptation to the position of the center of gravity

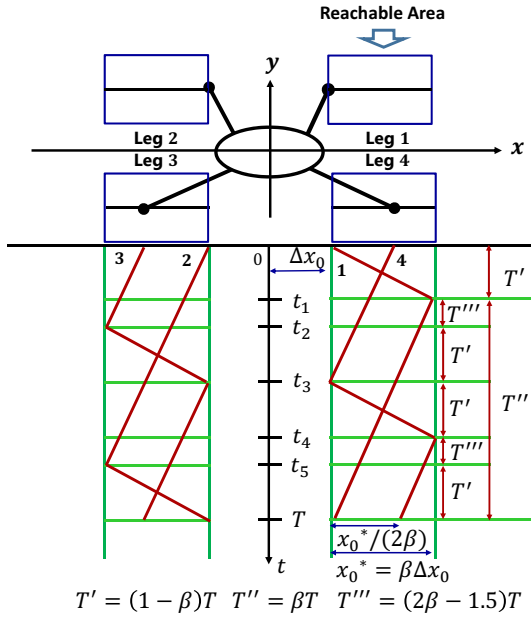


Figure 4: Gait diagram for  $x$ -directional standard gait

standard gait. In Figure 4, the blue rectangle is the reachable area of a leg. Standard gait is a gait in which the duty ratios of all the legs are equal in planar walking, the reference positions of the respective legs are symmetrically arranged with respect to the traveling direction, and the phase difference between the left and right legs is 0.5. When the robot realizes standard gait on a horizontal plane, the robot always realizes walking while maintaining static stability. However, with duty ratio  $\beta$  being 0.75,  $T_{SM}$  is zero at the moment when the free leg is switched.

### 3.2 Adaptive Gait

Figure 5 shows the robot standing on a slope. In Figure 5, the distance  $d$  between the point projecting the center of gravity on the slope and the point where the center of gravity is perpendicular to the slope is expressed as follows.

$$d = h \tan \theta \quad (14)$$

When the robot walks in Figure 5, a large load acts on the legs in a low position; when the leg becomes free, the tumble stability margin decreases. As a result, there is a possibility that the robot may tumble. Thus, adaptive gait prevents the robot from tumbling by maintaining the tumble stability margin by shifting the main body to the upper side of the slope by  $d$  (Figure 6) [8].

Figure 7 shows the gait diagram of adaptive gait, in which the main body is translated  $\Delta x$  in the  $x$  direction. By realizing this gait, the legged robot can walk stably on the slope. Here, a blue rectangle in Figure 7 is the reachable area. However, the legs are outside the reachable areas as the body is translated by  $\Delta x$ . It is for this reason that adaptive gait is not always possible. It is impossible to move the leg outside of this reachable region, where manipulability becomes zero. To solve this problem, we apply adaptive gait that considers the reachable area as shown in Figure 8. In Figure 8, we can see that the stroke of the leg decreases. Hence, adaptive gait, by taking into consideration the reachable area, keeps the tumble stability margin larger than that of standard gait, while preventing the leg from moving out of the reachable area by reducing the stride.

### 3.3 Sway Compensation Gait

Previously, sway compensation gait was proposed [9]. This gait enables the robot to walk more stably during dynamic motion by adjusting the acceleration of the body in the  $y$  axis direction. In this study, we apply this gait and make the robot more stable during static walking. In other words, by moving the main body semi-statically, the projected point of the center of gravity of the robot remains inside the support polygon. Figure 9 shows the gait di-

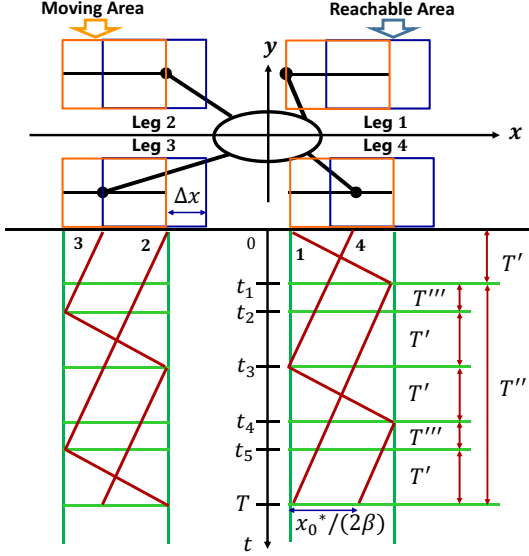


Figure 7: Gait diagram for  $x$ -directional adaptive gait

agram of sway compensation gait. The gait diagram of sway compensation gait in the  $x$  axis direction is the same as Figure 4. Then, Figure 9 shows the gait diagram in the  $y$  axis direction. In sway compensation gait, the body is moved left and right beforehand in the quadruped support phase. Therefore, sway compensation gait is able to prevent the tumble stability margin from being zero in the swing phase.

### 3.4 Hybrid Gait

In adaptive gait and sway compensation gait, by moving the body of the robot with respect to the slope, the tumble stability of the robot is maintained during slope walking. However, in both gaits the reachable area depends on the hardware of the walking robot, and this area determines the limits of each gait. For that reason, it is necessary to have a gait that can maximize utilization of the leg's reachable area and movement on a steeper slope. In this study, we therefore propose a gait called hybrid gait that combines both adaptive and sway compensation gaits. This is a gait in which the body translates in the  $x$  axis direction, which is the walking direction with respect to the slope, and the body swings to the right and left in the quadruped support phase. This prevents the tumble stability margin from becoming zero. It is for this reason that hybrid gait allows for slope walking.

## 4 SIMULATION ANALYSIS OF SLOPE WALKING

In this section, we examine the effectiveness of each gait by simulation. We performed gait analysis on the robot as shown in Figure 10. The joint arrangement of the robot prototype is the same as Figure 3 and  $L_1 = 2.9$  [cm],  $L_2 =$

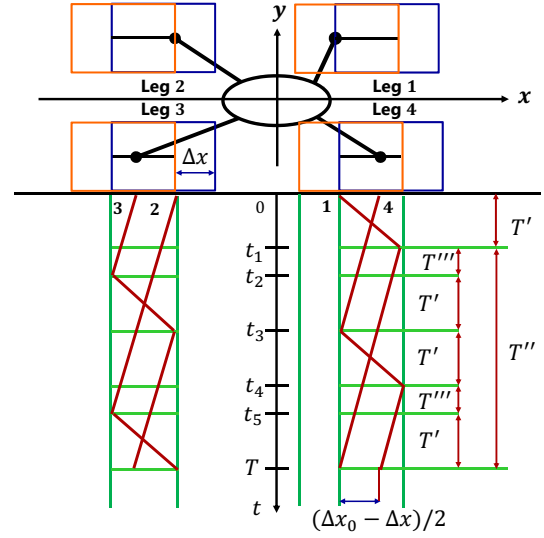


Figure 8: Gait diagram for  $x$ -directional adaptive gait considering manipulability

5.6 [cm],  $L_3 = 14.1$  [cm]. Furthermore, we define the mass of the body, link 1, link 2, and link 3 as  $m_0$ ,  $m_1$ ,  $m_2$ , and  $m_3$ , respectively, where  $m_0 = 676$  [g],  $m_1 = 95$  [g],  $m_2 = 110$  [g],  $m_3 = 9$  [g]. In addition, we set gait parameters as  $T = 11$  [s],  $\beta = 0.8$ ,  $\Delta x_0 = 5.0$  [cm], and  $h = 11.3$  [cm]. In adaptive gait and sway compensation gait, the swinging displacement of the body is set to 4.0 cm. In hybrid gait, the body is swung forward by 4.0 cm and left and right by 4.0 cm.

### 4.1 Comparison of Manipulability

In this study, manipulability does not depend on slope angle. Figure 11 shows time histories of minimum manipulability when each gait was executed for one cycle. In Figure 11, the manipulability of standard gait is at a maximum, and the manipulability of hybrid gait is relatively small. As a result, tumble stability is improved at the expense of manipulability. However, hybrid gait can make more use of the leg's reachable area compared with adaptive gait and sway compensation gait. This has a correlation with the displacement capable of swinging the body of the robot, and the swingable displacement also increases as the reachable area increases. Consequently, although hybrid gait is considered to be an unfavorable gait from the viewpoint of manipulability, it is more probable that it will enable more stable walking than other gaits, as its swingable displacement amount is large.

### 4.2 Comparison of Tumble Stability Margins

We simulate adaptive gait, sway compensation gait, and hybrid gait on a 23-degree slope for one cycle, and evaluate the time histories of tumble stability margin as shown in Figure 12. We can confirm that the tumble stability margin becomes a small value in the swing phase and a large

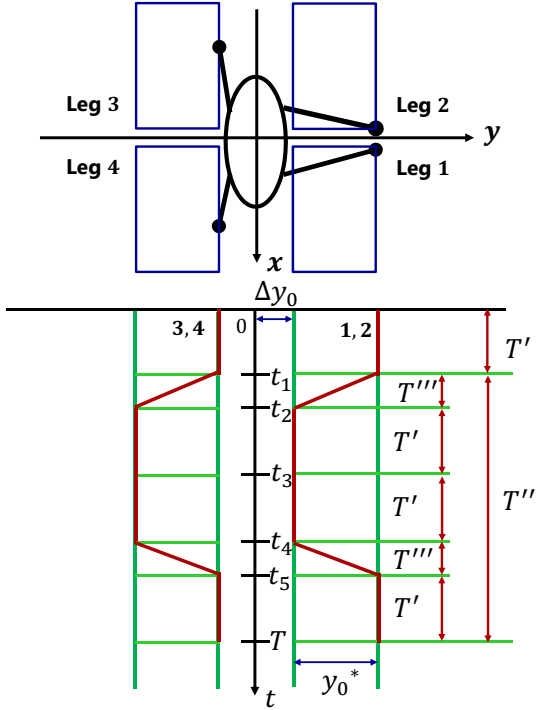


Figure 9: Gait diagram in an y-directional sway compensation gait

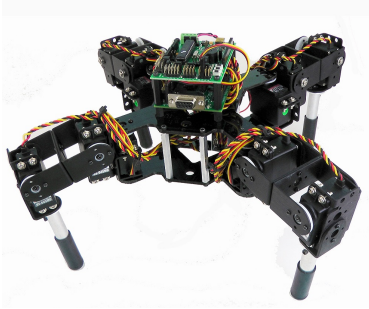


Figure 10: Quadruped robot ©Lynxmotion Inc.

value in the support phase. In particular, we can confirm that the values of the tumble stability margins of adaptive gait and sway compensation gait were zero around 3.2 s when the leg 3 becomes a free leg. Hence, the robot is unstable at this time. On the other hand, for hybrid gait, the tumble stability margin did not equal zero at one cycle of gait. Consequently, the robot could stably walk on the slope when using hybrid gait.

## 5 EXPERIMENTAL ANALYSIS OF SLOPE WALKING

In this section, we examine the effectiveness of each gait on a real robot system. We evaluate the tumble stability of the robot when each gait is applied using the robot shown in Figure 10. Gait parameters are set to the same value as

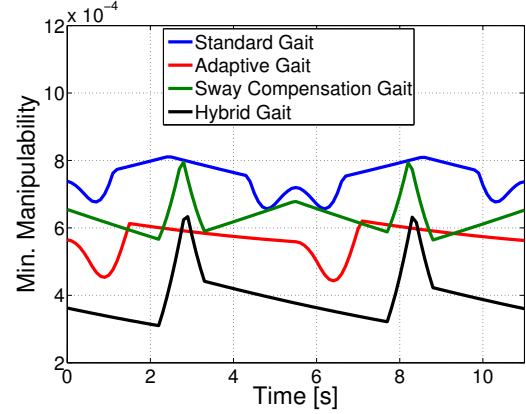


Figure 11: Time histories of manipulability of gaits

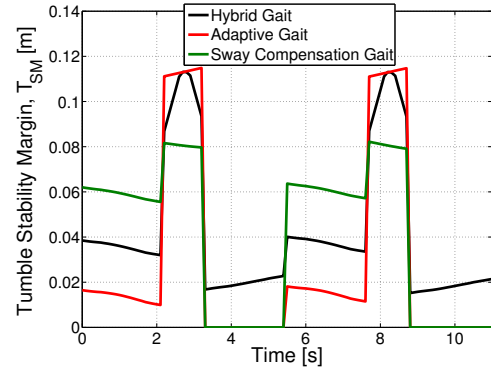


Figure 12: Simulation results of time histories of the tumble stability margins of gaits on a 23-degree slope

in the simulation. In the experiment, the behavior of the robot was recorded using a motion capture system.

### 5.1 Relation Between Gait and Tumble Stability Margin

We determine the y axis in Figure 5 according to the right-handed system. We define the pitch angle as the angle that the direction of the right screw makes with the y axis when the axis of rotation is negative. The pitch angular velocity of each gait was recorded on a 23-degree slope, and the result is shown in Figure 13.

As shown in Figure 13, the pitch angular velocities of adaptive gait and sway compensation gait have large values, and the tumbling phenomenon of the robot starts at around 3.2 s, at which time leg 3 becomes a free leg. Figure 14 shows the state of adaptive gait when the robot walks on a 23-degree slope. In Figure 14, we can see that leg 1 loses contact with the ground at 4.0 s. Thus, when the tumble stability margin became zero, a moment causing the robot to overturn was generated, and it was confirmed experimentally that the robot was dynamically unstable. On the other hand, the pitch angular velocity of the robot at the time of the hybrid gait showed a rela-

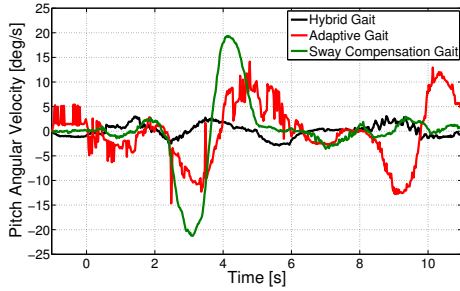


Figure 13: Experimental results of time histories of pitch angular velocity of gaits on a 23-degree slope

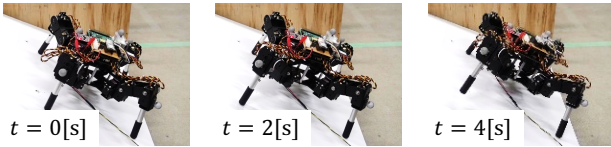


Figure 14: Adaptive gait on a 23-degree slope

tively small value with respect to adaptive gait and sway compensation gait, and the robot walked steadily. This is confirmed in Figure 15. Accordingly, it was possible to validate the usefulness of hybrid gait for slope walking from the experiment.

## 6 BENCHMARK FOR DESIGN OPTIMIZATION

In this section, we discuss the design guidelines of a free-climbing robot having a better ability to walk on uneven ground from the relation between the tumble stability margin and manipulability when changing the link ratio of the leg. By evaluating manipulability and tumble stability margin, it is possible to quantitatively evaluate the ratio of the links for stable slope walking as well as not causing gait failure.

For the simulation, the total of the lengths of link 2 and link 3 of the robot in Figure 3 was constant, and the regular gait was executed on the plane. We define the ratio of link length as  $r = L_2/L_3$ . Figure 16 shows the relation between the ratio of link length and tumble stability margin. In Figure 16, as the link ratio increases, that is,  $L_2$  increases with respect to  $L_3$ , it can be confirmed that the tumble stability margin increases. This is because link 2 is more important for increasing the area of the support polygon compared to link 3. The length of link 3 projected on the ground is shorter, owing to the trigonometric representation of the length between joint 2 and joint 3, whereas link 2 is affected only by joint 2. Therefore, in Figure 16, when considering the tumble stability margin, it is shown that the longer the length of link 2 is with respect to the length of link 3, the better is the tumble stability.

Next, as shown in Figure 17, we discuss the relation

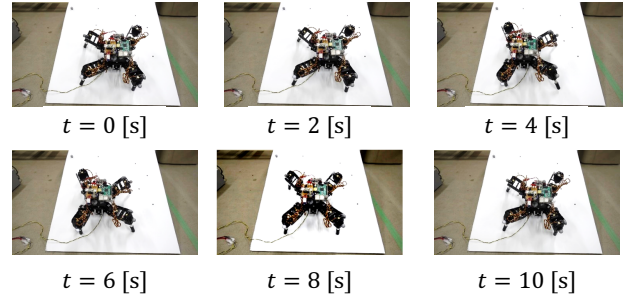


Figure 15: Hybrid gait on a 23-degree slope

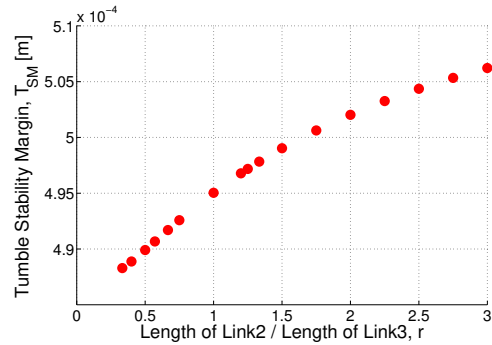


Figure 16: Relation between the ratio of link length and tumble stability margin

between the ratio of link length and manipulability. Figure 17 shows that the manipulability with respect to the link ratio is a convex function with a peak at 1.33. This is because in Eq. (12), when  $L_2$  increases,  $L_3$  decreases. From Eq. (12), it can be seen that the sum of the lengths of link 2 and link 3 is constant. Hence, the peak is shown at a certain link ratio.

Here, from Figure 16 and Figure 17, the Pareto front, which is a set of Pareto optimal solutions, is shown in Figure 18. We generated the Pareto front using the ranking method. The Pareto front can be an optimal solution in the multi-objective optimization problem. Accordingly, it is necessary to select one of the Pareto optimal solutions from the Pareto front based on the target robot. For example, because our target is reliable exploration in lunar and planetary exploration, it is considered that, if the tumble stability margin is as high as possible, it is difficult for the robot to tumble. In that case, we should select the Pareto optimal solution at the top left with the highest tumble stability margin in Figure 18.

## 7 CONCLUSION

In this paper, we presented a new gait, hybrid gait, for free-climbing on lunar planetary cliff faces. In hybrid gait, the main body of the robot translates in the walking direction and to the right and left. We analyzed walking stability of each gait during slope walking based on the tumble

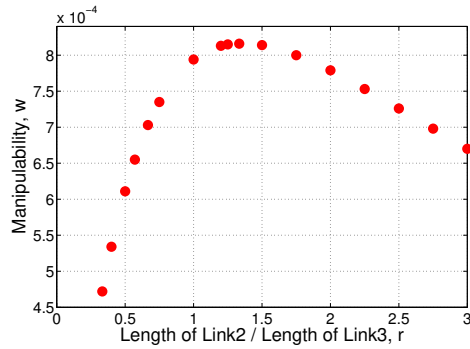


Figure 17: Relation between the ratio of link length and manipulability

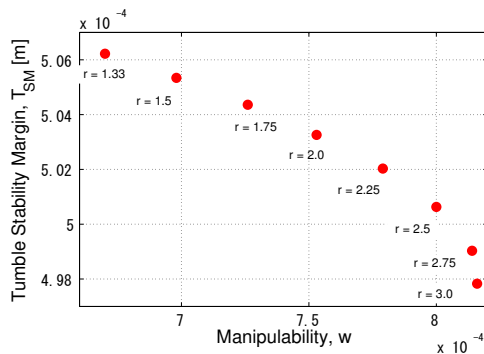


Figure 18: Pareto front of manipulability and tumble stability margin

stability margin and manipulability with numerical simulations and experiments. We verified the tumble stability of hybrid gait and confirmed that hybrid gait is more stable than conventional gaits, including adaptive gait and sway compensation gait. Furthermore, we provided a design guideline for a quadruped robot for slope walking on a slope based on the tumble stability margin and manipulability.

In future work, we expect to generate gaits in uneven environments where grippable points are limited using model predictive control. Moreover, we expect to enhance the autonomy of the robot using SLAM in order to plan the path to the destination.

## References

- [1] J. Haruyama et al., Possible Lunar Lava Tube Skylight Observed by SELENE Cameras, *Geophysical Research Letter*, vol. 36, issue 21, L21206(doi:10.1029/2009GL040635), 2009.
- [2] S. Squyres et al., Exploration of Victoria Crater by the Mars Rover Opportunity, *Science*, vol. 324, pp. 1058-1061, 2009.
- [3] K. Nagaoka et al., Passive Spine Gripper for Free-Climbing Robot in Extreme Terrain, *IEEE Robotics and Automation Letters*, vol. 3, issue 3, pp. 1765-1770, 2018.
- [4] A. Parness et al., LEMUR 3: A Limbed Climbing Robot for Extreme Terrain Mobility in Space, *2017 IEEE International Conference on Robotics and Automation*, pp. 5467-5473, 2017.
- [5] R. B. McGhee and A. A. Frank, On the Stability Properties of Quadruped Creeping Gaits, *Mathematical Biosciences*, vol. 3-3, pp. 331-351, 1968.
- [6] K. Yoneda and S. Hirose, Tumble Stability Criterion of Integrated Locomotion and Manipulation, *Proceedings of 1996 IEEE/RSJ International Conference on Intelligent Robots and Systems*, pp. 870-876, 1996.
- [7] T. Yoshikawa, Manipulability of robotic mechanisms, *International Journal of Robotics Research*, vol. 4, issue 2, pp. 3-9, 1985.
- [8] H. Adachi et al., Adaptive Gait for Quadruped Walking Robot Using Force Sensor, *Intelligent Autonomous Systems (edited by F. Groen et al.)*, IOS PRESS, Amsterdam, Netherlands, pp. 54-63, 1993.
- [9] R. Kurazume, T. Hasegawa, and K. Yoneda, The Sway Compensation Trajectory for a Biped Robot, *Proceedings of 2003 IEEE International Conference on Robotics Automation*, pp. 925-931, 2003.